

Operational Optimization to Maximize Dynamic Range in EXCLAIM Microwave Kinetic Inductance Detectors

Trevor M. Oxholm¹ · Eric R. Switzer² · Emily M. Barrentine² · Thomas Essinger-Hileman² · James P. Hays-Wehle² · Philip D. Mauskopf³ · Omid Noroozian² · Maryam Rahmani² · Adrian K. Sinclair³ · Ryan Stephenson³ · Thomas R. Stevenson² · Peter T. Timbie¹ · Carolyn Volpert⁴ · Eric Weeks³

the date of receipt and acceptance should be inserted later

Abstract Microwave Kinetic Inductance Detectors (MKIDs) are highly scalable detectors that have demonstrated nearly background-limited sensitivity in the far-infrared from high-altitude balloon-borne telescopes and space-like laboratory environments. In addition, the detectors have a rich design space with many optimizable parameters, allowing high sensitivity measurements over a wide dynamic range. For these reasons, MKIDs were chosen for the Experiment for Cryogenic Large-Aperture Intensity Mapping (EXCLAIM), a balloon-borne telescope targeting nearly background-limited performance in a high-altitude atmospheric environment from 420-540 GHz. We describe MKID optimization in the specific context of EXCLAIM and provide general results that apply to broader applications. Extending the established approach of tone frequency tracking, we show that readout power optimization enables significant, further improvement in dynamic range.

Keywords MKID, Telescope, Far-infrared Detector

1 Introduction

MKIDs are pair-breaking superconducting microwave resonators capable of highly sensitive detection of radiation, with applications ranging from millimeter waves to X-rays^{6,27,19}. Arrays of numerous MKID detectors can be multiplexed on a single transmission line²⁵ and are highly tunable to maximize sensitivity to a wide range of optical loading, making them ideal for use in terrestrial, suborbital, and space-based telescopes²⁴. MKIDs operate through

E-mail: Trevor M. Oxholm
oxholm@wisc.edu

¹Department of Physics, University of Wisconsin-Madison, Madison, WI 53706, USA

²NASA-Goddard Space Flight Center, Greenbelt, MD 20771, USA

³Department of Physics and School Of Earth and Space Exploration, Arizona State University, Tempe, AZ 85287, USA

⁴Department of Astronomy, University of Maryland, College Park, MD 20742, USA

the kinetic inductance effect, whereby energetic photons absorbed in a superconducting thin film break Cooper pairs, altering the inductance and resistance of the film. A single feedline can contain a comb of superconducting resonant circuits, each responding in amplitude and phase to an optical power delivered to the MKID.

MKID characteristics are tuned both by the geometry and materials, and dynamically as a function of their readout. The resonator geometry, including the active volume and the coupling capacitance, can be chosen to maximize sensitivity. The readout system permits additional detector optimization during operation by tuning the frequency and readout power transmitted to each detector. These readout optimizations can be performed uniquely for each detector and optical power, significantly increasing the dynamic range. This tunability is especially advantageous in spectroscopy, where the optical power varies widely across individual channels. In contrast, TESs can be designed to operate at higher optical power by increasing the saturation power through increased leg conduction, and compensating Joule power to target operating conditions. Higher conduction increases the intrinsic phonon noise¹⁹, making it difficult to achieve operation at high optical power without compromising noise at low optical power.

EXCLAIM⁴ is a balloon-borne cryogenic telescope featuring an aluminum MKID array and designed to demonstrate the line intensity mapping technique¹⁴ to obtain tomographic maps of extragalactic carbon monoxide and singly-ionized carbon emission, which may be used to infer the cosmic star formation history³. EXCLAIM features a set of six μ Spec spectrometers-on-a-chip with resolving power $R = 512$ read out in a 3.25-3.75 GHz microwave band²⁰ by a Xilinx RFSoc.

MKIDs have already demonstrated nearly background-limited performance in balloon^{18,11} and space-like¹ backgrounds in the far-infrared. Like other balloon- and space-based mid- to far-infrared missions, EXCLAIM detectors must accommodate a wide range of background loads spanning three orders of magnitude. MKIDs proposed for next-generation space instruments^{9,16} require high sensitivity over loads ranging from three⁹ to five² orders of magnitude, owing to the wide variety of science cases targeted by a single instrument. While the EXCLAIM mission does not require sensitivity to the brightest background loads, it will provide a valuable testbed for dynamic range optimization for future far-IR missions.

This study describes the optimization of the EXCLAIM MKID design over a wide range of background loads and the underlying device physics for general MKID applications. We focus on optimizing the readout system with a purely model-based approach, which can support dynamic range optimization during operation. Throughout, we simplify the model by choosing a single signal modulation frequency of 1 Hz and constant quasiparticle pair-breaking efficiencies, and we describe how these effects may be accounted for in the discussion section.

2 MKID sensitivity to a widely-varying background

The anticipated incident background load for EXCLAIM ranges from $P_{\text{opt}} \approx 0.1$ to 100 fW at the input of the spectrometer throughout the 420–540 GHz passband, with strong frequency-to-frequency variation driven by narrow atmospheric emission lines subject to low pressure broadening in the upper atmosphere⁴. Once the flight stabilizes, observations occur at 45° elevation at an altitude of ~ 34 km. Hence, dynamic range requirements apply to temporally stable loading rather than requiring significant real-time response. The space background is one to two orders of magnitude below the dark windows in upper atmospheric emission in the EXCLAIM band. Light passes through a cold stop to minimize stray light, then through

Parameter	Symbol	Parameter type	Value
Resonator volume	V	Design choice	$374 \mu\text{m}^3$
Dark resonator frequency	ν_0	Design choice	3.5 GHz
Coupling quality factor	Q_c	Design choice	2.3×10^5
Residual quality factor	Q_{i0}	Material	1.75×10^6
Kinetic inductance fraction	α	Material/Design	0.775
Readout qp generation efficiency	η_{read}	Material	9.24×10^{-4}
Amplifier temperature	T_{amp}	Design choice	4.1 K
TLS exponent	α_{TLS}	Material	-0.69
TLS spectral density at 1 kHz	$S_{0,\text{TLS}}$	Material	$1.49 \times 10^{-16} \text{ Hz}^{-1}$
TLS photon number	N_{TLS}	Material	241
Critical temperature	T_c	Material	1.33 K
Bath temperature	T_{bath}	Operational	100 mK
Read tone frequency	ν_{read}	Operational	variable
Read tone power	P_{read}	Operational	variable

Table 1: MKID design reference parameters for the EXCLAIM detector array. MKID performance is determined by the resonator film’s material parameters, design choices, and operational parameters. Material parameters in our model are based on lab measurements of Al CPW resonators fabricated at NASA-Goddard. For simplicity, we assume that the bath temperature is fixed.

the lenslet-coupled spectrometer, then into the MKID array. We estimate antenna efficiency (to the input of the spectrometer formed by the cold stop) $\eta_{\text{ant}} = 0.85$ and detector efficiency (through the cold stop to the detectors) of $\eta_{\text{det}} = 0.23$. Throughout, P_{opt} and NEP are defined at the cold stop (incident on the spectrometer lenslet) rather than at the detector in the on-chip spectrometer.

Assuming a model similar to Zmuidzinas²⁷ and Mauskopf¹⁹ with MKID design parameters shown in Tab. 1, we calculate the total NEP per detector through

$$\text{NEP}_{\text{tot}}^2 = \text{NEP}_{\text{opt}}^2 + \text{NEP}_{\text{gen}}^2 + \text{NEP}_{\text{rec}}^2 + \text{NEP}_{\text{amp}}^2 + \text{NEP}_{\text{TLS}}^2, \quad (1)$$

representing the total, optical, quasiparticle generation and recombination, amplifier, and two-level system (TLS) noise, respectively. Throughout, we assume frequency readout and signal modulation at a nominal frequency $f_{\text{mod}} = 1 \text{ Hz}$. The dominant sources of noise depend on the level of background radiation, which we specify in three regimes:

Low-background Loads: for low absorbed optical power, the detector NEP is typically dominated by generation noise and TLS noise, where the latter only affects readout in the frequency direction. Generation noise is caused by an increase in the number of quasiparticles from thermal phonons and readout photons, while TLS noise is produced by two-level systems at the boundaries of dielectric layers in the film. The NEP of these contributions is

$$\text{NEP}_{\text{gen}}^2 + \text{NEP}_{\text{TLS}}^2 = 4(\Gamma_{\text{th}} + \Gamma_{\text{read}}) \left(\frac{d\Gamma}{dP_{\text{opt}}} \right)^{-2} + S_{\text{TLS}} \left(\frac{dx}{dP_{\text{opt}}} \right)^{-2}, \quad (2)$$

where Γ_{th} and Γ_{read} are the quasiparticle generation rates due to thermal phonons and readout photons, respectively, and dx is the differential fractional frequency shift due to changes in optical power. We model the readout generation rate as $\Gamma_{\text{read}} = \eta_{\text{read}} P_{\text{read}}^{\text{abs}} / \Delta$, with $P_{\text{read}}^{\text{abs}}$ the absorbed readout power and $\Delta = 1.764 k_B T_c = 180 \text{ meV}$ the gap energy, where T_c is the critical temperature. We assume a constant η_{read} , though generally it may depend on the optical and readout powers (see Discussion below). Within the TLS noise term, $S_{\text{TLS}} = S_{0,\text{TLS}}(f_{\text{mod}}/\nu_{\text{TLS}})^{\alpha_{\text{TLS}}} \delta_{\text{TLS}}$ is the TLS power spectral density with $\nu_{\text{TLS}} = 1 \text{ kHz}$ pivot, and

$\delta_{\text{TLS}} = \tanh[h\nu_{\text{read}}/(2k_B T)]^{1.5} \cdot (N_{\text{ph}} + N_{\text{TLS}})^{-1/2}$ describes losses due to TLS, with $N_{\text{ph}} = P_{\text{read}}^{\text{abs}} Q_i (2\pi h \nu_{\text{read}}^2)^{-1}$ the number of readout photons. Here, ν_{read} is the microwave readout frequency and h is Planck's constant. This form matches measurements of resonators with $\nu_{\text{read}} = 3.4$ GHz by Gao⁸ suggesting $S_{\text{TLS}} \sim T^{-1.5}$ for $T > 100$ mK. $dx/dP_{\text{opt}} \equiv R_x \propto \tau_{\text{qp}}/V$ is the frequency responsivity describing variations in resonator frequency due to the kinetic inductance effect, and $d\Gamma/dP_{\text{opt}} = q/h\nu$, where $q \equiv h\nu\eta_{\text{pb}}/\Delta$ is the number of quasiparticles produced per photon, and η_{pb} describes the pair-breaking efficiency, evaluating to $\eta_{\text{pb}} = 0.57$ when the photon energy $> 2\Delta$, as is the case for the optical frequencies of interest here¹⁵. Note that noise from single-quasiparticle interactions may also contribute to generation noise due to e.g. magnetic field flux trapping⁷.

Photon Background-limited Loads: the background-limited noise-equivalent power (NEP) for unpolarized radiation at the input of an incoherent detector such as an MKID is²⁶

$$\text{NEP}_{\text{opt}}^2 = 2h\nu P_{\text{opt}} + \frac{2P_{\text{opt}}^2}{B}, \quad (3)$$

where ν is the frequency of the incident radiation, B is the spectrometer optical bandwidth per channel, and P_{opt} is the incident optical power.

Recombination noise due to optically-generated quasiparticles produces an additional irreducible source of noise¹⁷. $\text{NEP}_{\text{rec}}^2 \approx 4h\nu q^{-1} P_{\text{opt}}$ in the case that quasiparticle generation is dominated by optical photons. For EXCLAIM we find that $\text{NEP}_{\text{rec}}/\text{NEP}_{\text{photon}} \approx \sqrt{2q^{-1}}$, producing a $\sim 23\%$ increase in NEP compared to the photon background at 480 GHz.

High-background Loads: for high optical power, amplifier noise dominates the EXCLAIM detector noise, with NEP given by

$$\text{NEP}_{\text{amp}}^2 = \frac{k_B T_{\text{amp}}}{P_{\text{read}}^{\text{feed}}} \left(\left| \frac{\partial S_{21}}{\partial x} \right| R_x \right)^{-2} = \frac{k_B T_{\text{amp}}}{P_{\text{read}}^{\text{feed}}} (\chi_a Q_i R_x)^{-2}. \quad (4)$$

where $\chi_a = 2(Q_r^2 Q_i^{-1} Q_c^{-1}) (1 + 2Q_r x)^{-1}$ is the absorption efficiency, with x the fractional frequency detuning, which equals zero when the readout tone frequency is on resonance. Here, the resonator quality factor is $Q_r^{-1} = Q_c^{-1} + Q_i^{-1}$, and the χ_a is maximized when $Q_i = Q_c$. χ_a represents the fraction of the delivered readout power $P_{\text{read}}^{\text{feed}}$ that is absorbed by the MKID, as $P_{\text{read}}^{\text{abs}} = \chi_a P_{\text{read}}^{\text{feed}}$.

3 Readout tone-tracking and readpower optimization

Several design parameters (e.g. V and Q_c) may be used to optimize detectors for a given application but are functions of the resonator geometry, and therefore cannot be optimized operationally. On the other hand, the readout system may implement in-situ NEP optimization as a function of optical power. The readout system enables two techniques:

Resonance tone-tracking: the tracking of each readout tone to be exactly on-resonance, i.e. $x=0$ for χ_a in Eqn. 4, minimizing amplifier noise. Without tone-tracking, we assume the readout tone equals the resonance frequency under a nominal optical loading and that the resonator can move away from this fixed tone under changing optical power (Fig. 1, right). Note that a similar dependence occurs when reading out in dissipation quadrature, where $\text{NEP}_{\text{amp,diss}} \propto \chi_a^{-1}$.

Readout power optimization: an adjustable readout power $P_{\text{read}}^{\text{feed}}$ delivered to each detector, minimizing the NEP per frequency channel. For low optical powers, a decrease in

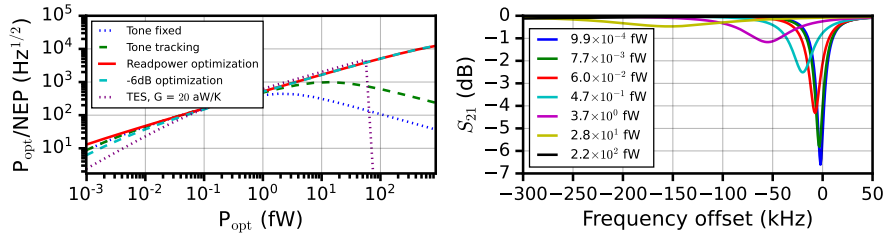


Fig. 1: Simulated comparison between the three operational regimes. Left: instantaneous dynamic range, defined as the ratio of the optical power to the total NEP, akin to the signal-to-noise for one second of integration time. Right: magnitude of transmission S_{21} for a selection of incident optical power across the EXCLAIM band.

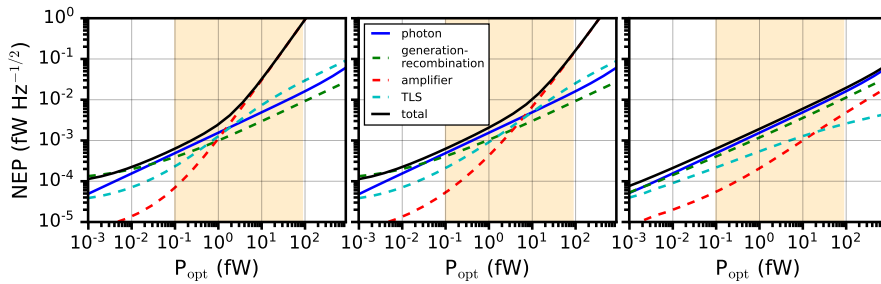


Fig. 2: Simulated NEP curves for three cases: (left) fixed readpower without tone-tracking, (center) fixed readpower with tone-tracking, and (right) optimized readpower with tone-tracking. The shaded orange region represents the range of anticipated incident optical power for the EXCLAIM mission. In the left two plots, the readpower is fixed to minimize NEP at $P_{\text{opt}} = 0.15 \text{ fW}$, whereas the right plot optimizes at all input optical powers. In the left plot, the lack of tone-tracking causes a frequency mismatch, thereby increasing amplifier noise at high input optical power.

$P_{\text{read}}^{\text{feed}}$ leads to a decrease in NEP_{gen} , provided the resonator is cold enough for thermal quasi-particle generation and TLS noise to be subdominant. For high optical powers, an increase in $P_{\text{read}}^{\text{feed}}$ suppresses amplifier noise, up to the regime where the resonator response begins to bifurcate²² or otherwise display signs of nonlinear response.

These in-situ optimizations are significant for EXCLAIM because they maximize the sensitivity per channel without uniquely fabricating each detector to its anticipated flight loading. In EXCLAIM's expected flight operation, the tone-tracking and readpower optimization steps will be performed once the altitude stabilizes through measurements of quality factor and resonator frequencies as a function of several readpowers, requiring roughly a minute of data. We anticipate only requiring this optimization once, after the altitude stabilizes. Approaches for real-time optimization of readpower in response to optical power are deferred to future work, but may measure derivatives between tones on and near resonance. A low-power pulsed optical reference emitter will enable periodic responsivity checks²³.

Within the proposed RFSOC-based readout design for EXCLAIM²¹, a PID loop style tone tracking algorithm can be applied after the digital down conversion stage in a time-division multiplexed fashion. Two PIDs will be used, each with an estimated resource utilization of 3 DSP48 multipliers, 2 FIFOs of length 512, and 5 adders. This uses only a fraction of the resources compared to the front-end FFT.

In the low optical power regime where noise is dominated by quasiparticle generation-recombination and TLS, the readpower that minimizes noise also maximizes the internal quality factor $Q_i = (Q_{qp}^{-1} + Q_{TLS}^{-1} + Q_{i0}^{-1})^{-1}$. Here, Q_{i0} is an empirical residual quality factor, $Q_{TLS} = 2.61 \times 10^4 \delta_{TLS}^{-1}$ is the dissipation due to two-level systems with δ_{TLS} defined after Eqn. 2, and $Q_{qp} \propto \delta n_{qp}^{-1}$ is the dissipation due to quasiparticles in the film, which decreases with an increased number of quasiparticles. Note that readpower optimization differs from the typical operational procedure to maximize χ_a by setting $Q_i = Q_c$. Utilizing readpower optimization, a design with Q_c lower than Q_i can achieve near-ideal noise performance while also providing robustness to changes in optical loading, realized quality factors, and resonance-finding. Because Q_i can be measured directly through S_{21} in a readpower sweep, this technique is less time- and computation-intensive compared to measuring and minimizing the noise directly. The relation between maximal Q_i and minimal NEP breaks down for high optical powers where amplifier noise dominates; in this case, increasing the readpower reduces the noise. For EXCLAIM, however, these optically bright, high-noise channels do not contribute as strongly to the extragalactic science signal, so the Q_i optimization step will suffice. More work will be needed to define the readpower optimization routine in future missions requiring higher sensitivities to brighter sources.

Based on these techniques, we analyze the noise performance of the EXCLAIM detector design under three regimes: (i) fixed tone (i.e. the tone frequency is fixed to the resonance under nominal loading) with fixed readpower; (ii) resonance tone-tracking with fixed readpower; (iii) resonance tone-tracking with optimized readpower. While the first two regimes have been demonstrated in laboratory and operational environments¹³, the active readout power optimization represents a new technique; previous approaches have optimized the readout power by e.g. setting it to -6 dB below the bifurcation power threshold¹¹. In the model presented here, setting the feedline readpower -6 dB below the bifurcation threshold and including tone tracking leads to a 26% increase in NEP compared to our optimization method for 0.01 fW loads and a 108% increase for $10\times$ lower loads, while 1000 fW loads are within 1%.

Fig. 1 (left) shows the dynamic range performance and Fig. 2 shows the noise contributions in each operational regime, with minimum loads set a decade lower than the EXCLAIM minimum. In the case of the fixed readpower, $P_{read}^{feed} = 4.8$ fW ($P_{read}^{abs} = 2.4$ fW) minimizes the NEP at $P_{opt} = 0.15$ fW, representing a typical dark channel in the EXCLAIM passband. The case with optimized readpower scales approximately as $P_{read}^{feed} \approx 1.6$ fW + $27 P_{opt}$. A basic TES sensitivity model is also shown, including noise from phonons and photons, as well as saturation. Here, we follow the model of Mauskopf¹⁹ taking $G = 20$ aW/K and $F_{link} = 0.6$.

4 Discussion

We have investigated and modeled the physical effects of MKID optimizations through the readout system, including resonance tone-tracking and the optimization of the readout power as a function of optical power. These conclusions have several caveats that we will study through future measurements. In particular, nonlinear behavior has been observed in MKIDS

with high incident background loads, due to bifurcation and nonlinear heating. In Goddard AI CPW test devices, this behavior has tentatively been observed at higher readpowers than the range described here. Future models can employ quasiparticle kinetic equations^{5,10} representing the local heating and cooling of quasiparticles, resulting in non-constant values for η_{read} and, to a lesser extent, η_{pb} ¹². The simple model used here agrees with readpower sweeps in the critical regime across the maximum of the quality factor.

Second, the quasiparticle lifetime may limit sensitivities at lower power levels and rapid signal variations. As a function of signal modulation frequency f_{mod} , the finite quasiparticle lifetime leads to increased TLS noise as $\text{NEP}_{\text{TLS}} \propto f_{\text{mod}}^{\alpha_{\text{TLS}}/2}$ and decreased responsivities through the multiplication of the responsivity R_r (following Eqn. 4) by $[1 + (2\pi f_{\text{mod}} \tau_{\text{qp}})^2]^{-1}$, leading to an increase in TLS and amplifier NEP. Note that τ_{qp} is inversely proportional to the number of quasiparticles in this model. However, for low-quality films or low quasiparticle densities, this quantity may saturate, resulting in a maximum lifetime τ_{max} ²⁷. Furthermore, the quasiparticle free-decay time may also limit sensitivities for f_{mod} , though τ_{qp} provides a more stringent constraint for the MKIDs described here.

With careful accounting for these caveats, the readpower optimization and tone-tracking techniques we describe can provide nearly background-limited sensitivity over a wide range of optical power. This tunability provides an incentive for developing MKIDs for instruments requiring a wide dynamic range, including proposed space telescopes. In the EXCLAIM band, the simpler technique of setting P_{read} to 6dB below the bifurcation approximates the optimal noise performance on all but the darkest loads. The widely-ranging background anticipated for the EXCLAIM mission will offer a testbed for these techniques.

Acknowledgements This work was supported by a 5-year NASA Astrophysics Research and Analysis (APRA 17-APRA17-0077) grant and NASA-Goddard Internal Research and Development funds, and TMO acknowledges support from the NASA-Goddard internship program and the UW-Madison graduate program.

References

1. J. Baselmans, J. Bueno, S. J. Yates, O. Yurduseven, N. Llombart, K. Karatsu, A. Baryshev, L. Ferrari, A. Endo, D. Thoen, et al. A kilo-pixel imaging system for future space based far-infrared observatories using microwave kinetic inductance detectors. *Astronomy & Astrophysics*, 601:A89, 2017.
2. C. M. Bradford, B. A. Cameron, B. D. Moore, S. Hailey-Dunsheath, E. G. Amatucci, D. C. Bradley, J. A. Corsetti, D. T. Leisawitz, M. J. DiPirro, J. G. Tuttle, et al. Origins survey spectrometer: revealing the hearts of distant galaxies and forming planetary systems with far-ir spectroscopy. *Journal of Astronomical Telescopes, Instruments, and Systems*, 7(1):011017, 2021.
3. C. Carilli and F. Walter. Cool gas in high-redshift galaxies. *Annual Review of Astronomy and Astrophysics*, 51:105–161, 2013.
4. G. Cataldo, P. A. Ade, C. J. Anderson, A. Barlis, E. M. Barrentine, N. G. Bellis, A. D. Bolatto, P. C. Breysse, B. T. Bulcha, J. A. Connors, et al. Overview and status of exclaim, the experiment for cryogenic large-aperture intensity mapping. In *Ground-based and Airborne Telescopes VIII*, volume 11445, page 1144524. International Society for Optics and Photonics, 2020.
5. J.-J. Chang and D. Scalapino. Nonequilibrium superconductivity. *Journal of Low Temperature Physics*, 31(1):1–32, 1978.

6. P. K. Day, H. G. LeDuc, B. A. Mazin, A. Vayonakis, and J. Zmuidzinas. A broadband superconducting detector suitable for use in large arrays. *Nature*, 425(6960):817–821, 2003.
7. D. Flanigan, B. R. Johnson, M. H. Abitbol, S. Bryan, R. Cantor, P. Day, G. Jones, P. Mauskopf, H. McCarrick, A. Miller, et al. Magnetic field dependence of the internal quality factor and noise performance of lumped-element kinetic inductance detectors. *Applied Physics Letters*, 109(14):143503, 2016.
8. J. Gao. *The physics of superconducting microwave resonators*. PhD thesis, California Institute of Technology, 2008. <http://thesis.library.caltech.edu/2530>.
9. J. Glenn, C. M. Bradford, E. Rosolowsky, R. Amini, K. Alatalo, L. Armus, A. J. Benson, T.-C. Chang, J. Darling, P. K. Day, et al. Galaxy evolution probe. *Journal of Astronomical Telescopes, Instruments, and Systems*, 7(3):034004, 2021.
10. D. Goldie and S. Withington. Non-equilibrium superconductivity in quantum-sensing superconducting resonators. *Superconductor Science and Technology*, 26(1):015004, 2012.
11. S. Gordon, A. Sinclair, P. Mauskopf, G. Coppi, M. Devlin, B. Dober, L. Fissel, N. Galitzki, J. Gao, J. Hubmayr, et al. Preflight detector characterization of blast-tng. *Journal of Low Temperature Physics*, 200(5):400–406, 2020.
12. T. Guruswamy, D. Goldie, and S. Withington. Quasiparticle generation efficiency in superconducting thin films. *Superconductor Science and Technology*, 27(5):055012, 2014.
13. J. R. Hoh, A. Sinclair, and R. Stephenson. Maximizing dynamic range of microwave kinetic inductance detectors through high-speed tone tracking. In J. Zmuidzinas and J.-R. Gao, editors, *Millimeter, Submillimeter, and Far-Infrared Detectors and Instrumentation for Astronomy X*, volume 11453. International Society for Optics and Photonics, SPIE, 2020. doi: 10.1117/12.2559899. URL <https://doi.org/10.1117/12.2559899>.
14. E. D. Kovetz, M. P. Viero, A. Lidz, L. Newburgh, M. Rahman, E. Switzer, M. Kamionkowski, J. Aguirre, M. Alvarez, J. Bock, et al. Line-intensity mapping: 2017 status report. *arXiv preprint arXiv:1709.09066*, 2017.
15. A. Kozorezov, A. Volkov, J. Wigmore, A. Peacock, A. Poelaert, and R. Den Hartog. Quasiparticle-phonon downconversion in nonequilibrium superconductors. *Physical Review B*, 61(17):11807, 2000.
16. D. Leisawitz, E. G. Amatucci, L. N. Allen, J. W. Arenberg, L. Armus, C. Battersby, J. M. Bauer, P. Beltran, D. J. Benford, D. Burgarella, et al. Origins space telescope: baseline mission concept. *Journal of Astronomical Telescopes, Instruments, and Systems*, 7(1): Art–No, 2021.
17. A. Lowitz, E. Barrentine, S. Golwala, and P. Timbie. A comparison of fundamental noise in kinetic inductance detectors and transition edge sensors for millimeter-wave applications. *Journal of Low Temperature Physics*, 176(3):504–510, 2014.
18. S. Masi, P. De Bernardis, A. Paiella, F. Piacentini, L. Lamagna, A. Coppolecchia, P. Ade, E. Battistelli, M. Castellano, I. Colantoni, et al. Kinetic inductance detectors for the olimpo experiment: in-flight operation and performance. *Journal of Cosmology and Astroparticle Physics*, 2019(07):003, 2019.
19. P. Mauskopf. Transition edge sensors and kinetic inductance detectors in astronomical instruments. *Publications of the Astronomical Society of the Pacific*, 130(990):082001, 2018.
20. M. Mirzaei, E. M. Barrentine, B. T. Bulcha, G. Cataldo, J. A. Connors, N. Ehsan, T. M. Essinger-Hileman, L. A. Hess, S. H. Moseley, J. W. Mugge-Durum, et al. μ -spec spec-

- trometers for the exclaim instrument. In *Millimeter, Submillimeter, and Far-Infrared Detectors and Instrumentation for Astronomy X*, volume 11453, page 114530M. International Society for Optics and Photonics, 2020.
21. R. Stephenson. paper in preparation.
 22. L. Swenson, P. Day, B. Eom, H. Leduc, N. Llombart, C. McKenney, O. Noroozian, and J. Zmuidzinas. Operation of a titanium nitride superconducting microresonator detector in the nonlinear regime. *Journal of Applied Physics*, 113(10):104501, 2013.
 23. E. R. Switzer, E. M. Barrentine, G. Cataldo, T. Essinger-Hileman, P. A. Ade, C. J. Anderson, A. Barlis, J. Beeman, N. Bellis, A. D. Bolatto, et al. Experiment for cryogenic large-aperture intensity mapping: instrument design. *Journal of Astronomical Telescopes, Instruments, and Systems*, 7(4):044004, 2021.
 24. G. Ulbricht, M. De Lucia, and E. Baldwin. Applications for microwave kinetic induction detectors in advanced instrumentation. *Applied Sciences*, 11(6):2671, 2021.
 25. J. van Rantwijk, M. Grim, D. van Loon, S. Yates, A. Baryshev, and J. Baselmans. Multiplexed readout for 1000-pixel arrays of microwave kinetic inductance detectors. *IEEE Transactions on Microwave Theory and Techniques*, 64(6):1876–1883, 2016.
 26. J. Zmuidzinas. Thermal noise and correlations in photon detection. *Applied optics*, 42(25):4989–5008, 2003.
 27. J. Zmuidzinas. Superconducting microresonators: Physics and applications. *Annu. Rev. Condens. Matter Phys.*, 3(1):169–214, 2012.